AIAA Guidance, Navigation, and Control Conference and Exhibit
15 - 18 August 2005, San Francisco, California

AIAA 2005-6455

Integrated Sliding Mode Autopilot-Guidance for Dual Control Missiles

Moshe Idan*
Technion - Israel Institute of Technology, Haifa, 32000, Israel

Tal Shima† and Oded M. Golan‡
RAFAEL, Haifa 31021, Israel

An integrated autopilot and guidance algorithm is developed, using the sliding mode control approach, for a missile with forward and aft control surfaces. Based on guidance considerations, the zero effort miss (ZEM), encountered in differential games guidance solutions, is used as one of the sliding variables in the proposed control scheme. The dual control configuration provides an additional degree of freedom in the integrated design. This degree of freedom is exploited by introducing a second sliding surface, selected based on autopilot design considerations. Restraining the system to the ZEM surface guarantees zero miss distance, while remaining on the second surface provides a damped response. The performance of the integrated dual controller is evaluated using a two-dimensional nonlinear simulation of the missile lateral dynamics and relative kinematics, assuming first order dynamics for the target evasive maneuvers. The simulation results validate the design approach of using ZEM and the flight-control based sliding surfaces to attain high accuracy interceptions.

Nomenclature

a	acceleration
A, B, C, G	state space model matrices
$f_{(\cdot)}(\cdot)$	missile nonlinear aerodynamics function
$\boldsymbol{f}, \boldsymbol{g}$	vector functions
H	matrix used to determine the SMC control signal
I	moment of inertia
$\mathscr{L}$	Lyapunov function candidate
L	lift force
$L_{(\cdot)}$	lift force derivative
$\mathscr{M}$	SMC uncertainty controller parameter matrix
M	pitch moment
$M_{(\cdot)}$	pitch moment derivative
m	mass
q	pitch rate
r	range
t, t_{go}	time, time-to-go
U_m	saturation limit
V	speed
$X - M - Z$	body reference frames

*Associate Professor, Faculty of Aerospace Engineering; AIAA Associate Fellow; moshe.idan@technion.ac.il
†Currently NRC visiting scientist at the Control and Optimization Branch, Air Vehicles Directorate, Air Force Research Laboratories, Room 304, Building 146, Wright-Patterson AFB, OH 45433; AIAA Senior Member; shima_tal@yahoo.com
‡Chief Systems Engineer, P.O.B. 2250, Department 35; AIAA Senior Member; odedgol@rafael.co.il

$X-O-Z$	inertial reference frame
$\boldsymbol{x}$	state vector
Z	zero effort miss
z	target-missile relative displacement normal to the initial LOS
$\bar{(\cdot)}$	approximation/model
α	angle of attack
$\Delta\phi$	maneuver phase
ΔT	target maneuver period
$\Delta, \bar{\Delta}$	modeling errors and their bounds
δ	control surface deflection angle
$\boldsymbol{\delta}$	vector of control surface deflections: canard and tail
$\boldsymbol{\eta}$	augmented missile state vector
γ	flight path angle
λ	angle between the temporary and initial LOS
μ	SMC uncertainty controller parameter
Φ	transition matrix
ψ	function of individual contributions in computing the ZEM
σ	sliding variable
$\boldsymbol{\sigma}$	sliding vector
τ	time constant
θ	pitch angle

Subscripts

0	initial values
bf	body frame parallel to the inertial frame
br	body rotating frame
c	canard
E	evasive target
EN	evader component perpendicular to the LOS
eq	equivalent control
I	inertial coordinate frame
kin	kinematics
M	missile
MN	missile component perpendicular to the LOS
q	pitch rate
r	radial, along the LOS
t	tail
Z	zero effort miss
α	angle of attack
δ_c	canard control
δ_t	tail control
λ	perpendicular to the LOS

Superscripts

B	body contribution to the aerodynamics force and moment
c	command
max	maximum

Abbreviations

c.g.	center of gravity
LOS	line of sight
SMC	sliding mode control
ZEM	zero effort miss

I. Introduction

DESIGNING an interceptor missile imposes tradeoffs between conflicting requirements. For example, to obtain the required agility in a high-end air-to-air interception engagement a canard configuration is often employed due to the improved homing performance;[1] the canard fins, located in the front part of the fuselage, generate an aerodynamic force that is in the same direction as the required maneuvering force, thus generating (neglecting servo dynamics) an immediate response in the correct direction. However, if the missile is to perform sharp initial turns, canard control may limit its performance due to aerodynamic saturation at high angles of attack, and tail control may be preferred. By using both canard and tail controls a favorable design compromise can be obtained to provide enhanced performance.

The additional degree of freedom offered by the dual control system requires special consideration in the guidance and autopilot design. In many studies the focus was on controlling the airframe. A sliding mode approach[2,3] with a linear strategy for blending the two control actions was suggested in several works.[4–6] Neural networks were used in Ref. 7 for the design of adaptive nonlinear control for an agile missile with forward and aft reaction control systems and aerodynamic tail control surfaces. In Ref. 8 the coefficient diagram method was used for an all aerodynamic tail fins and canard configuration. In recent papers the focus was different; it was on designing the end-game guidance strategy for such a dual control missile. The approach was based on the assumption that the additional degree of freedom can be best utilized by providing the guidance law with the capability of optimally imparting the commands to the two controls. In Ref. 9 the missile control limits were treated indirectly, by incorporating penalties on the use of the controls in the linear quadratic optimal control and differential games formulation of the problem, while in Ref. 10 the control bounds were explicitly taken into account. The performance of these control schemes was investigated using high order noisy simulation in Ref. 11 and the superiority over classical designs was advocated.

Integrated flight control and guidance law design may enhance the endgame performance of the interceptor by accounting for the coupling between the control and guidance dynamics. Moreover, in a dual control configuration it will inherently make use of the additional degree of freedom. In such designs, the entire guidance and control loop is stated as a solution to a finite horizon control problem, instead of the common approach treating the inner autopilot loop as an unrealistically infinite horizon one. The integrated design also allows for a more effective use of the information on the missile states in the guidance problem formulation, as opposed to using only the missile acceleration data in separated guidance loop designs. In Ref. 12, a game theoretic approach was used for the design of an integrated autopilot-guidance linear controller, which minimizes the final miss distance and control energy under worst case target maneuvers and measurements uncertainty. The feedback linearization method[13] was used in Ref. 14 in a finite horizon problem setting. In Ref. 15, a state dependent Riccati differential equation approach was used for designing the integrated controller. Using a 6 degrees-of-freedom simulation it was shown that the integrated controller provides improved miss distance statistics compared to the conventional two-loop design practice.

In recent papers,[16,17] the sliding mode control (SMC) methodology was applied to the design of an integrated guidance-autopilot controller. The usefulness of SMC comes from being a nonlinear, robust control design approach enabling to maintain stability and performance in the presence of modeling errors. Simplified controllers are obtained using SMC by converting a tracking problem of an n-th order dynamical system into a first order stabilization problem. This approach leads to satisfactory performance in the presence of bounded but otherwise arbitrary parameter inaccuracies and model uncertainties. In Ref. 16 it was applied to obtain a two-loop design, utilizing backstepping and high order SMC methods. In the outer SMC-like guidance loop, a sliding surface that depends on the line of sight (LOS) rate was defined with the missile pitch rate used as a virtual control. The inner loop was designed to robustly enforce the pitch rate command of the outer loop in the presence of uncertainties. Numerical simulation was used to demonstrate the performance and robustness of the integrated design in tracking an evasive maneuvering target in the presence of atmospheric disturbances and uncertainty in the plant and actuator dynamics. In Ref. 17 SMC was used for the derivation of an integrated autopilot-guidance controller, utilizing the zero-effort miss (ZEM) distance as its single sliding surface. The performance of the integrated controller was compared with that of two different two-loop designs and the superiority of the integrated design was demonstrated especially in severe scenarios where spectral separation between guidance and flight control, implicitly assumed in any two-loop design, is not valid.

In the present paper the SMC methodology is used for the design of an integrated guidance-autopilot controller for a missile controlled by two aerodynamic surfaces. Compared to the single control case, the

additional degree of freedom requires the definition of an additional sliding surface. This surface is selected using flight-control considerations, such as improved stability and shaped/damped response.

In the next section the actual, approximate, and linearized kinematics and dynamics models of the interception problem are introduced. Next, the integrated guidance-autopilot controller is synthesized, along with the definition of the two sliding surfaces used for the design. Then, the interaction between the surfaces and the homing performance is analyzed using non-linear simulations. Concluding remarks are offered in the last section.

II. Model Derivation

A skid-to-turn cruciform, roll stabilized, missile with forward and aft maneuver surfaces is considered. The motion of such a missile can be separated into two perpendicular channels. Consequently, the guidance and control of a target interception problem can be treated as planar in each of these channels. We first present the full nonlinear kinematics and dynamics equations of the interception problem, which will serve for analysis. Then, approximate dynamics, that will be used for the design of the nonlinear sliding mode guidance-autopilot controller, are presented. Finally, linearized equations are derived, which will serve as the basis for the selection of the SMC sliding surfaces.

A. Non Linear Kinematics and Dynamics

1. Engagement Kinematics

In Fig. 1 a schematic view of the planar endgame geometry is shown, where $X_I - O_I - Z_I$ is a Cartesian inertial reference frame. We denote the missile and the evasive target by the subscripts M and E, respectively. The speed, normal acceleration, and flight path angles are denoted by V, a and γ, respectively; the range between the adversaries is r, and λ is the angle between the initial and current LOS.

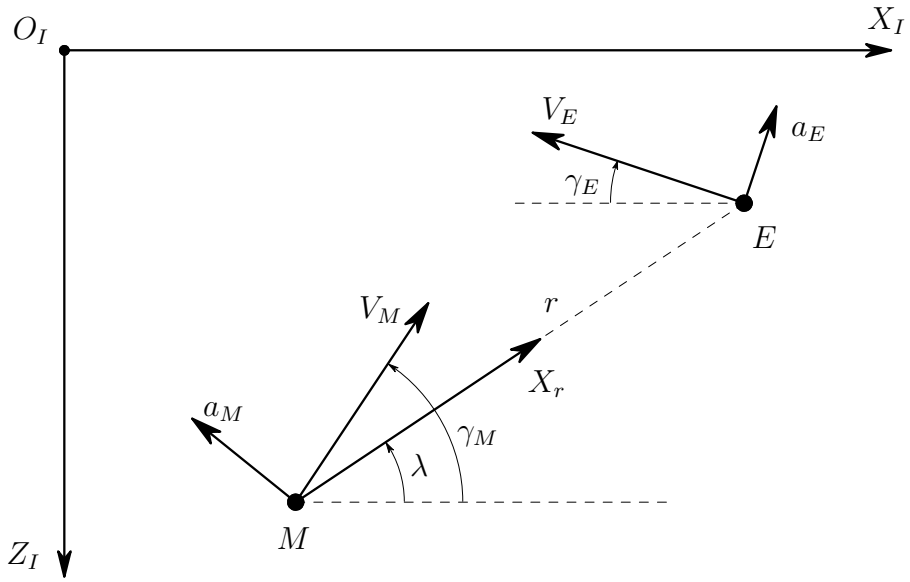

Figure 1. Planar engagement geometry.

Neglecting the gravitational force, the engagement kinematics, expressed in a polar coordinate system (r, λ) attached to the missile, is

$$\dot{r} = V_r \tag{1a}$$

$$\dot{\lambda} = V_\lambda / r \tag{1b}$$

where the closing speed V_r is

$$V_r = -\left[V_M \cos\left(\gamma_M - \lambda\right) + V_E \cos\left(\gamma_E + \lambda\right)\right] \tag{2}$$

and the speed perpendicular to the LOS is

$$V_\lambda = -V_M \sin(\gamma_M - \lambda) + V_E \sin(\gamma_E + \lambda) \tag{3}$$

The interception duration or the time-to-go, t_{go}, used in the subsequent derivations, is approximated by

$$t_{go} = -r/V_r \ , \quad V_r < 0 \tag{4}$$

During the end-game (the time of interest in our analysis) we assume that $V_r < 0$, and the engagement terminates when V_r crosses zero.

2. Target Dynamics

In this formulation, it is assumed that the evading target is moving at a constant speed and performs lateral maneuvers only. The lateral target dynamics are approximated by a first order model

$$\dot{\gamma}_E = a_E/V_E \tag{5a}$$
$$\dot{a}_E = \left(a_E^c - a_E\right)/\tau_E \tag{5b}$$

where τ_E is the time constant of the target dynamics and a_E^c is the target maneuver command. We assume that $|a_E^c| \leq a_E^{max}$, where a_E^{max} is the maximum target acceleration command.

The target acceleration perpendicular to LOS, routinely used in guidance logic synthesis, is given by

$$a_{EN} = a_E \cos(\gamma_E + \lambda) \tag{6}$$

3. Missile Dynamics

The missile planar dynamics are expressed using the coordinate systems presented in Fig. 2. $X_{bf} - M - Z_{bf}$ is parallel to the inertial frame $X_I - O_I - Z_I$, with its origin located at the missile's center of gravity (c.g.). It is used to express the missile attitude relative to the inertial frame. The missile equations of motion are derived in the rotating body fixed coordinate frame $X_{br} - M - Z_{br}$, where the X_{br} axis is aligned with the missile's longitudinal axis. It is assumed that during the end-game, the time of interest in our analysis, the missile speed is constant. Thus, the planar missile dynamics are given by

$$\dot{\alpha} = q - L(\alpha, \delta_c, \delta_t)/(mV_M) \tag{7a}$$
$$\dot{q} = M(\alpha, q, \delta_c, \delta_t)/I \tag{7b}$$
$$\dot{\theta} = q \tag{7c}$$
$$\dot{\delta}_c = \left(\delta_c^c - \delta_c\right)/\tau_c \tag{7d}$$
$$\dot{\delta}_t = \left(\delta_t^c - \delta_t\right)/\tau_t \tag{7e}$$

where the state variables α, q and θ are, respectively, the angle of attack, pitch rate and pitch attitude of the missile. m and I are its mass and moment of inertia, respectively. δ_c and δ_t are, respectively, the deflection angles of the missile canard and tail aerodynamic surfaces. These surfaces are controlled by actuators, modeled by first order dynamics with time constants τ_c and τ_t. M is the pitch moment acting on the missile; and L is the lift force generated by the missile and its control surfaces. The aerodynamic forces and moments are nonlinear, partly unknown functions of the related variables, in particular α, q, δ_c and δ_t.

The missile flight path angle γ_M and acceleration perpendicular to the LOS, a_{MN}, are given by

$$\gamma_M = \theta - \alpha \tag{8}$$
$$a_{MN} = a_M \cos(\gamma_M - \lambda) \tag{9}$$

Here, a_M is the missile acceleration perpendicular to its velocity vector, given by

$$a_M = L(\alpha, \delta_c, \delta_t)/m \tag{10}$$

In modeling the missile dynamics, we assume that the lift and the aerodynamic pitch moment in Eqs. (7) are generated by the missile body and the control surfaces. This is modeled by

$$L/m = L_\alpha^B f_1(\alpha) + L_{\delta_c} f_2(\alpha + \delta_c) + L_{\delta_t} f_3(\alpha + \delta_t) \tag{11a}$$
$$M/I = M_\alpha^B f_4(\alpha) + M_q q + M_{\delta_c} f_5(\alpha + \delta_c) + M_{\delta_t} f_6(\alpha + \delta_t) \tag{11b}$$

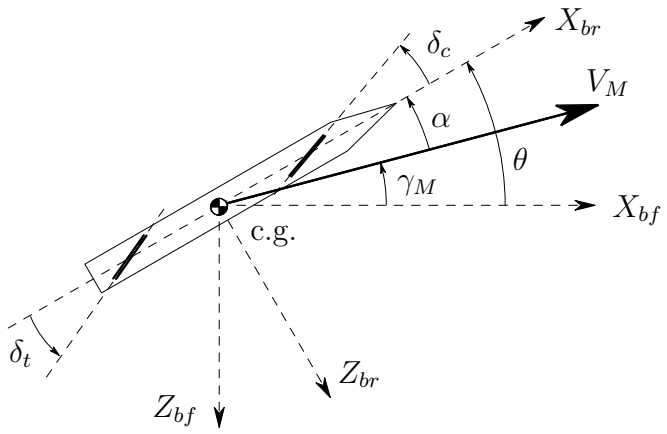

Figure 2. Missile coordinate systems.

where

$$L_\alpha^B = L_\alpha - L_{\delta_c} - L_{\delta_t} \tag{12a}$$
$$M_\alpha^B = M_\alpha - M_{\delta_c} - M_{\delta_t} \tag{12b}$$

$L_{(\cdot)}$ and $M_{(\cdot)}$ denote the stability and control derivatives of the short period model; and $f_i(\cdot), i = 1, \ldots, 6$ express the nonlinear aerodynamic characteristics of the missile.

B. Approximate Dynamics

We assume that the true dynamics of the target and missile are unknown to the designer of the missile autopilot and guidance. Thus, only approximate dynamics can be used, imposing modeling errors. These approximations are discussed next.

1. Target

The true target dynamics are assumed to be related to the approximate first order linear model of Eq. (5b) by

$$\dot{a}_{EN} = \left(a_{EN}^c - a_{EN}\right)/\tau_E + \Delta_{aEN} \tag{13}$$

where the target acceleration command and the modeling error are assumed to be bounded by

$$|a_{EN}^c| \leq \bar{\Delta}_{aENc} \tag{14a}$$
$$|\Delta_{aEN}| \leq \bar{\Delta}_{aEN} \tag{14b}$$

2. Missile

The integrated controller, designed in the sequel, uses an approximation of the nonlinear model of Eqs. (7), (11), i.e.,

$$\dot{\alpha} = q - \left[\bar{L}_\alpha^B \bar{f}_1(\alpha) + \bar{L}_{\delta_c} \bar{f}_2(\alpha + \delta_c) + \bar{L}_{\delta_t} \bar{f}_3(\alpha + \delta_t)\right]/V_M + \Delta_\alpha \tag{15a}$$
$$\dot{q} = \bar{M}_\alpha^B \bar{f}_4(\alpha) + \bar{M}_q q + \bar{M}_{\delta_c} \bar{f}_5(\alpha + \delta_c) + \bar{M}_{\delta_t} \bar{f}_6(\alpha + \delta_t) + \Delta_q \tag{15b}$$
$$\dot{\delta}_c = \left(\delta_c^c - \delta_c\right)/\tau_c \tag{15c}$$
$$\dot{\delta}_t = \left(\delta_t^c - \delta_t\right)/\tau_t \tag{15d}$$

where $\bar{L}_{(\cdot)}$, $\bar{M}_{(\cdot)}$ and $\bar{f}_i(\cdot), i = 1, \ldots, 6$ are approximations of their respective quantities and functions. Δ_α and Δ_q express the modeling errors that are assumed to be bounded by

$$|\Delta_\alpha| \leq \bar{\Delta}_\alpha \tag{16a}$$
$$|\Delta_q| \leq \bar{\Delta}_q \tag{16b}$$

We assume no modeling errors on the actuators dynamics.

C. Linearized Kinematics and Dynamics

The definition of the sliding surfaces in the integrated guidance-autopilot design will be based on simplified kinematics and dynamics models. For that, it is assumed that during the endgame, the missile and target deviations from the collision triangle are small. Thus, linearization of the endgame kinematics, are performed around the initial LOS.[18] The linearized kinematics variables are depicted in Fig. 3, where the X-axis is aligned with the initial LOS. The approximate short-period linearized equations of motion are used for the missile dynamics.[19]

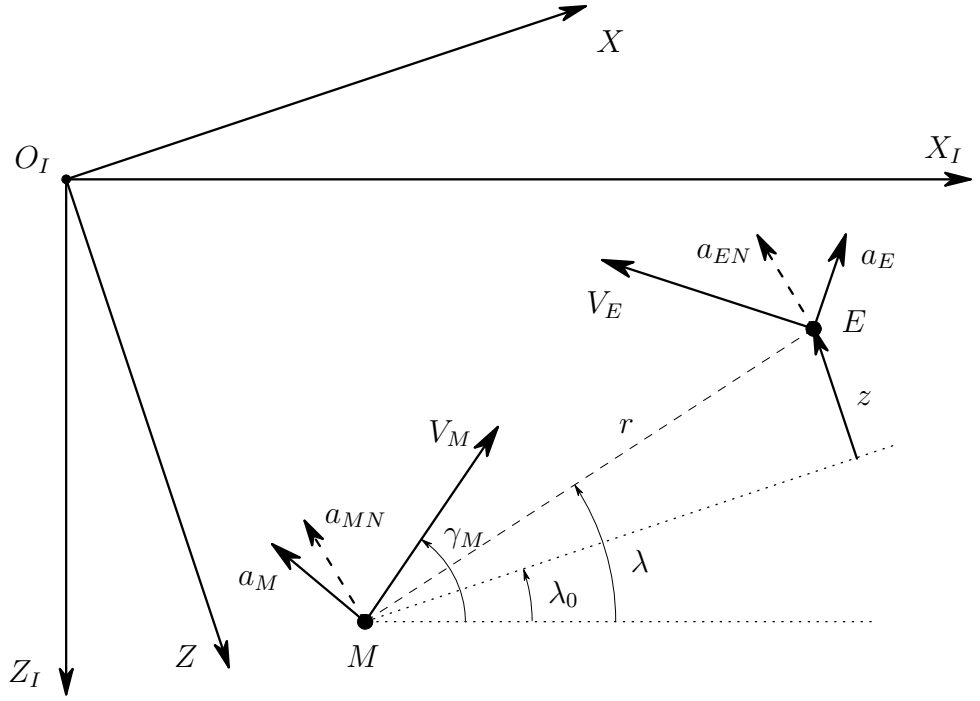

Figure 3. Linearized endgame kinematics

The state vector of the integrated guidance-autopilot problem is defined by

$$\boldsymbol{x} = \begin{bmatrix} z & \dot{z} & a_{EN} & \alpha & q & \delta_c & \delta_t \end{bmatrix}^T \tag{17}$$

where z is the relative displacement between the target and the missile normal to the initial LOS. Within the linear setting, a_{MN}, defined in Eq. (9), is approximated by

$$a_{MN} \approx a_M \cos\left(\gamma_{M_0} - \lambda_0\right) \tag{18}$$

where the subscript 0 denotes the initial value around which linearization has been performed. Thus, the missile acceleration normal to the initial LOS, a_{MN}, is given by

$$a_{MN} = C_M \begin{bmatrix} \alpha & q & \delta_c & \delta_t \end{bmatrix}^T \tag{19}$$

where

$$C_M = \begin{bmatrix} L_\alpha & 0 & L_{\delta_c} & L_{\delta_t} \end{bmatrix} \cos\left(\gamma_{M_0} - \lambda_0\right) \tag{20}$$

The equations of motion of the integrated dynamics are

$$\dot{\boldsymbol{x}} = A\boldsymbol{x} + B\boldsymbol{\delta}^c + Ga_{EN}^c \tag{21}$$

where

$$A = \begin{bmatrix} A_{kin} & A_{12} \\ [0]_{4\times 3} & A_M \end{bmatrix}, \quad A_{12} = \begin{bmatrix} [0]_{1\times 4} \\ -C_M \\ [0]_{1\times 4} \end{bmatrix}, \quad B = \begin{bmatrix} [0]_{3\times 2} \\ B_M \end{bmatrix} \tag{22}$$

$$G = \begin{bmatrix} 0 & 0 & 1/\tau_E & 0 & 0 & 0 & 0 \end{bmatrix}^T \tag{23}$$

and $[0]_{a\times b}$ denotes a matrix of zeros with appropriate dimensions. From the equations of relative motion normal to the initial LOS

$$A_{kin} = \begin{bmatrix} 0 & 1 & 0 \\ 0 & 0 & 1 \\ 0 & 0 & -1/\tau_E \end{bmatrix} \tag{24}$$

Using Eqs. (7) and (11) the linearized short period dynamics, coupled with the first order control surface actuation models of Eqs. (7d) and (7e), yield

$$A_M = \begin{bmatrix} -L_\alpha/V_M & 1 & -L_{\delta_c}/V_M & -L_{\delta_t}/V_M \\ M_\alpha & M_q & M_{\delta_c} & M_{\delta_t} \\ 0 & 0 & -1/\tau_c & 0 \\ 0 & 0 & 0 & -1/\tau_t \end{bmatrix}, \; B_M = \begin{bmatrix} 0 & 0 \\ 0 & 0 \\ 1/\tau_c & 0 \\ 0 & 1/\tau_t \end{bmatrix} \tag{25}$$

III. Integrated SMC Guidance-Autopilot Synthesis

The SMC design methodology entails three major steps: a) selection of a sliding manifold $\boldsymbol{\sigma} = 0$ to ensure stable desired dynamic characteristics of the system once in the sliding mode; b) computation of the equivalent control to impose $\dot{\boldsymbol{\sigma}} = 0$ once on the sliding surfaces, while using an approximate model of the system dynamics; and c) choosing an uncertainty controller to ensure stability and finite time convergence to the surfaces when $\boldsymbol{\sigma} \neq 0$.

A. Sliding Surfaces

The ZEM[18] is the expected miss distance computed using the homogenous solution of the associated linear engagement equations of motion. Its usefulness in missile guidance problems where the only state of importance is the miss distance, comes from reducing the n-dimensional guidance problem to a scalar one. Also, its dynamic equation depends only on the system inputs. The ZEM is dependent on the problem formulation and model. In a one-sided optimal control optimization problem it has the physical meaning of being the miss distance, if from the current time onwards the interceptor does not apply controls and the target performs the expected maneuver. In a two-sided differential game problem, ZEM is the miss distance, if from the current time onwards both players do not apply controls. In a recent study,[17] for a canard controlled missile (SISO problem), the differential game based ZEM was chosen as the single sliding surface for an integrated guidance-autopilot design. This choice does not require any assumption regarding the future maneuvers of the target. If the system response is maintained on this surface, it provides zero miss distance. Moreover, once on the surface, no control action is needed to ensure interception in the nominal linear case with perfect modeling and no target maneuvers. In a realistic nonlinear environment, with modeling errors and target maneuvers, the uncertainty control element of the SMC solution is designed to nullify deviations from the sliding surface in finite time.

The governing equation that is used to define the ZEM is the linearized Eq. (21). Due to the definition of ZEM, assuming that $\boldsymbol{\delta}^c = \begin{bmatrix} \delta_c^c & \delta_t^c \end{bmatrix}^T$ and a_{EN}^c are identically zero, the measurement-like equation of ZEM denoted by Z is

$$Z = C_Z \boldsymbol{x}\left(t_{go}\right) \tag{26}$$

where

$$C_Z = \begin{bmatrix} 1 & 0 & 0 & 0 & 0 & 0 & 0 \end{bmatrix} \tag{27}$$

To compute $\boldsymbol{x}\left(t_{go}\right)$, we introduce the transition matrix $\Phi\left(t_f, t\right)$, which, for the linear time invariant system of Eq. (21), is given by

$$\Phi\left(t_f, t\right) = \Phi\left(t_{go}\right) = \exp\left(A t_{go}\right) \tag{28}$$

Thus,

$$\boldsymbol{x}\left(t_{go}\right) = \Phi\left(t_{go}\right) \boldsymbol{x} \tag{29}$$

Using the expression of Eqs. (28) and (29) in Eq. (26), the ZEM is expressed as

$$\begin{aligned} Z &\triangleq C_Z \Phi\left(t_{go}\right) \boldsymbol{x} \\ &= z + \dot{z} t_{go} + a_{EN} \tau_E^2 \psi\left(t_{go}/\tau_E\right) \\ &\quad + \psi_\alpha\left(t_{go}\right) \alpha + \psi_q\left(t_{go}\right) q + \psi_{\delta_c}\left(t_{go}\right) \delta_c + \psi_{\delta_t}\left(t_{go}\right) \delta_t \end{aligned} \tag{30}$$

where

$$\psi(\zeta) = \exp(-\zeta) + \zeta - 1 \tag{31}$$

and $\psi_\alpha\left(t_{go}\right)$, $\psi_q\left(t_{go}\right)$, $\psi_{\delta_c}\left(t_{go}\right)$ and $\psi_{\delta_t}\left(t_{go}\right)$ are complicated functions of the system parameters and t_{go}, and hence of the kinematics variables.

Assuming small deviations from a collision triangle, the displacement z normal to the initial LOS can be approximated by $z \approx (\lambda - \lambda_0) r$. Differentiating with respect to time yields

$$z + \dot{z} t_{go} = -V_r t_{go}^2 \dot{\lambda} = V_\lambda t_{go} \tag{32}$$

Thus, the first two terms in Eq. (30) can be expressed as a function of the kinematics variables V_r, V_λ and r. The last four complicated terms of Eq. (30) can be obtained from the numerically computed transition matrix $\Phi\left(t_{go}\right)$ associated with A of Eq. (22). Using this together with the relationship obtained in Eq. (32), the ZEM of Eq. (30) is expressed as

$$Z = V_\lambda t_{go} + a_{EN} \tau_E^2 \psi\left(t_{go}/\tau_E\right) + C_Z \Phi\left(t_{go}\right) \boldsymbol{\eta} \tag{33}$$

where

$$\boldsymbol{\eta} = \begin{bmatrix} 0 & 0 & 0 & \alpha & q & \delta_c & \delta_t \end{bmatrix}^T \tag{34}$$

contains the missile variables of the state vector $\boldsymbol{x}$, pre-pended with zeros.

In the current two-input MIMO problem we seek an additional sliding surface to fully exploit the design degrees of freedom offered by the dual control configuration. The sought after surface should not interfere with the first surface, ensuring zero miss distance if the system is kept on it. Moreover, if possible it should not restrict the canard control, as it has been shown in several studies that it has a higher effect in enhancing the homing performance.[1,11,20] Thus, we choose the following sliding surface based on flight-control considerations, without explicitly referring to the canard control

$$\sigma_M = \bar{M}_\alpha^B \bar{f}_4(\alpha) + \bar{M}_{\delta_t} \bar{f}_6(\alpha + \delta_t) \tag{35}$$

The above expresses the angle of attack and tail contributions to the missile aerodynamic pitch moments, resulting from the approximate model of Eq. (15b). Since the missile is assumed stable this surface enforces the tail control to produce a moment equal to the one generated by the body, but in an opposite direction. Thus, missile response is damped, and trim is enforced provided there are no maneuver commands issued by the canard. The canard commands may be caused by guidance considerations, in order to remain on the $Z = 0$ surface.

In the sequel, the two sliding surfaces are grouped into the sliding vector $\boldsymbol{\sigma} = \begin{bmatrix} Z & \sigma_M \end{bmatrix}^T$.

B. Equivalent Controller

The equivalent controller is designed to maintain the system on the sliding surfaces, once those are attained. This is obtained by imposing $\dot{\boldsymbol{\sigma}} = 0$. Thus, the derivation of the equivalent controller will require a derivative of the sliding vector.

The time derivative of ZEM is given by

$$\begin{aligned} \dot{Z} &= \dot{V}_\lambda t_{go} + V_\lambda \dot{t}_{go} + \tau_E^2 \left[\dot{a}_{EN} \psi\left(t_{go}/\tau_E\right) + a_{EN} \psi'\left(t_{go}/\tau_E\right) \dot{t}_{go}\right] \\ &\quad + C_Z \left[\Phi'\left(t_{go}\right) \dot{t}_{go} \boldsymbol{\eta} + \Phi\left(t_{go}\right) \dot{\boldsymbol{\eta}}\right] \end{aligned} \tag{36}$$

where

$$\dot{V}_r = V_\lambda^2 / r + a_M \sin\left(\gamma_M - \lambda\right) + a_E \sin\left(\gamma_E + \lambda\right) \tag{37}$$

$$\dot{V}_\lambda = -V_\lambda V_r / r - a_M \cos\left(\gamma_M - \lambda\right) + a_E \cos\left(\gamma_E + \lambda\right) \tag{38}$$

$$\dot{t}_{go} = -1 + \dot{V}_r r / V_r^2 \tag{39}$$

and

$$\psi'\left(t_{go}/\tau_E\right) = \partial\psi\left(t_{go}/\tau_E\right)/\partial t_{go} = \left[t_{go}/\tau_E - \psi\left(t_{go}/\tau_E\right)\right]/\tau_E \tag{40}$$

$$\Phi'\left(t_{go}\right) = \partial\Phi\left(t_{go}\right)/\partial t_{go} = \Phi\left(t_{go}\right)A \tag{41}$$

Due to the structure of $\boldsymbol{\eta}$, its derivative $\dot{\boldsymbol{\eta}}$ used in Eq. (36) is given by Eqs. (15), pre-pended with three zero elements. This can be expressed by

$$\dot{\boldsymbol{\eta}} = \boldsymbol{f}\left(\boldsymbol{\eta}\right) + \Delta\boldsymbol{f}\left(\boldsymbol{\eta}\right) + B\boldsymbol{\delta}^c \tag{42}$$

where $\boldsymbol{f}\left(\boldsymbol{\eta}\right)$ are the known state dependent terms of Eqs. (15), while $\Delta\boldsymbol{f}\left(\boldsymbol{\eta}\right)$ contains the modeling errors Δ_α and Δ_q in its 4-th and 5-th elements, respectively. The matrix B is defined in Eq. (22).

The time derivative of the second surface is given by

$$\dot{\sigma}_M = \left[\bar{M}_\alpha^B \bar{f}_4'(\alpha)\right]\dot{\alpha} + \left[\bar{M}_{\delta_t}\bar{f}_6'(\alpha+\delta_t)\right]\left(\dot{\alpha}+\dot{\delta}_t\right) \tag{43}$$

where $\bar{f}_i'(\cdot), i = 4, 6$ denote the partial derivatives of the functions $\bar{f}_i(\cdot), i = 4, 6$ with respect to their respective arguments. In this equation, $\dot{\alpha}$ is computed using Eq. (15a) or, equivalently, equals the fourth element of $\boldsymbol{f}\left(\boldsymbol{\eta}\right) + \Delta\boldsymbol{f}\left(\boldsymbol{\eta}\right)$ in Eq. (42), i.e.,

$$\dot{\alpha} = C_\alpha \boldsymbol{f}\left(\boldsymbol{\eta}\right) + \Delta_\alpha \tag{44}$$

where $C_\alpha = \left[\begin{array}{ccccccc} 0 & 0 & 0 & 1 & 0 & 0 & 0 \end{array}\right]$.

The relations of Eqs. (13), (15d), (42) and (44) are used in Eqs. (36) and (43) to yield

$$\dot{\boldsymbol{\sigma}} = \boldsymbol{g} + \Delta\boldsymbol{g} + H\boldsymbol{\delta}^c \tag{45}$$

where

$$\begin{aligned} \boldsymbol{g} &= \left\{\begin{array}{c} \dot{V}_\lambda t_{go} + V_\lambda \dot{t}_{go} + a_{EN}\tau_E^2\left[\psi'\left(t_{go}/\tau_E\right)\dot{t}_{go} - \psi\left(t_{go}/\tau_E\right)/\tau_E\right] \\ \left[\bar{M}_\alpha^B \bar{f}_4'(\alpha) + \bar{M}_{\delta_t}\bar{f}_6'(\alpha+\delta_t)\right] C_\alpha \boldsymbol{f}\left(\boldsymbol{\eta}\right) - \left[\bar{M}_{\delta_t}\bar{f}_6'(\alpha+\delta_t)\right]\delta_t/\tau_t \end{array}\right\} \\ &+ \left\{\begin{array}{c} C_Z\Phi\left(t_{go}\right)\left[A\dot{t}_{go}\boldsymbol{\eta} + \boldsymbol{f}\left(\boldsymbol{\eta}\right)\right] \\ 0 \end{array}\right\} \end{aligned} \tag{46a}$$

$$\Delta\boldsymbol{g} = \left\{\begin{array}{c} \left(a_{EN}^c + \tau_E\Delta_{a_{EN}}\right)\tau_E\psi\left(t_{go}/\tau_E\right) + C_Z\Phi\left(t_{go}\right)\Delta\boldsymbol{f}\left(\boldsymbol{\eta}\right) \\ \left[\bar{M}_\alpha^B \bar{f}_4'(\alpha) + \bar{M}_{\delta_t}\bar{f}_6'(\alpha+\delta_t)\right]\Delta_\alpha \end{array}\right\} \tag{46b}$$

$$H = \left[\begin{array}{c} C_Z\Phi\left(t_{go}\right)B \\ \left[\begin{array}{cc} 0 & \bar{M}_{\delta_t}\bar{f}_6'(\alpha+\delta_t)/\tau_t \end{array}\right] \end{array}\right] \tag{46c}$$

The particular choice of the sliding surfaces ensures that the matrix H in Eq. (46c) is upper triangular with non-zero terms on the diagonal, and hence nonsingular. Using the bounds in Eqs. (14) and (16), the two elements of $\Delta\boldsymbol{g}$ can be bounded as

$$\left|\Delta g_i\right| \le \bar{\Delta}_{g_i}, \quad i = 1, 2 \tag{47}$$

In the absence of modeling errors and target maneuvers, once the system reaches the sliding surface it will remain on it using the equivalent control command $\boldsymbol{\delta}_{eq}^c$ given by

$$\boldsymbol{\delta}_{eq}^c = -H^{-1}\boldsymbol{g} \tag{48}$$

C. Uncertainty Controller

Modeling uncertainties and disturbances may cause the system to depart from the sliding surfaces. To accommodate these departures the equivalent controller is augmented by a second component, sometimes referred to as the *uncertainty controller*. The goal of this uncertainty controller is to drive the system to the sliding surface in finite time, while ensuring closed-loop stability. The design of the uncertainty controller is based on the approximate models of the system dynamics given in Eqs. (13)-(16). The kinematics model of Eqs. (1)-(3) is assumed to be known exactly.

The integrated guidance control logic is designed using the Lyapunov function candidate

$$\mathscr{L} = \frac{1}{2}\boldsymbol{\sigma}^T\boldsymbol{\sigma} \tag{49}$$

The time derivative of this Lyapunov function candidate is given by

$$\dot{\mathscr{L}} = \boldsymbol{\sigma}^T\dot{\boldsymbol{\sigma}} = \boldsymbol{\sigma}^T\left(\boldsymbol{g} + \Delta\boldsymbol{g} + H\boldsymbol{\delta}^c\right) \tag{50}$$

where the result in Eq. (45) was used for $\dot{\boldsymbol{\sigma}}$. The SMC controller is chosen to be

$$\boldsymbol{\delta}^c = \boldsymbol{\delta}^c_{eq} - H^{-1}\mathscr{M}\mathrm{sgn}(\boldsymbol{\sigma}) \tag{51}$$

The second term on the right hand side of Eq. (51) is the uncertainty controller, where $\mathscr{M} = \mathrm{diag}(\mu_1, \mu_2)$ is a diagonal 2×2 matrix, and $\mathrm{sgn}(\boldsymbol{\sigma}) = \begin{bmatrix}\mathrm{sgn}(\sigma_1) & \mathrm{sgn}(\sigma_2)\end{bmatrix}^T$. With this controller, the derivative of the Lyapunov function candidate becomes

$$\dot{\mathscr{L}} = \boldsymbol{\sigma}^T\left[\Delta\boldsymbol{g} - \mathscr{M}\mathrm{sgn}(\boldsymbol{\sigma})\right] = \sum_{i=1}^{2}\sigma_i\left[\Delta g_i - \mu_i\mathrm{sgn}(\sigma_i)\right] \tag{52}$$

Using the bounds in Eqs. (47), this derivative can be bounded by

$$\dot{\mathscr{L}} \leq -\sum_{i=1}^{2}|\sigma_i|\left(\mu_i - \bar{\Delta}_{g_i}\right) \tag{53}$$

Choosing

$$\mu_i > \bar{\Delta}_{g_i}, \quad i = 1, 2 \tag{54}$$

will guaranty a negative definite Lyapunov function derivative and hence convergence to the two-dimensional sliding manifold in finite time. Moreover, the values of $\mu_i, i = 1, 2$ could be tuned to emphasize the attraction of one sliding surface compared to the other. In a realistically noisy and uncertain interception environment, a boundary layer around the sliding surface can be employed to provide smooth control commands and to avoid chattering caused by the sgn function in Eq. (51).

IV. Performance Analysis

Performance of the proposed integrated guidance and control algorithm is evaluated through numerical simulations, incorporating the nonlinear models of Eqs. (1), (5) and (7). A sample run is first examined, followed by a Monte Carlo study.

A. Scenario

The numerical study was performed for a generic interceptor model, that is based on the missile control example introduced in Ref. 21 and utilized in Ref. 11. It is assumed that the target performs a square wave evasive maneuver with a period of ΔT and a phase of $\Delta\phi$ relative to the beginning of the simulation. The initial missile-target range was set to 1000 m. The initial missile velocity vector was aligned with the initial LOS. The target initial velocity vector is pointed 20 deg away from the initial LOS. An example of the engagement geometry and trajectories is plotted in Fig. 4.

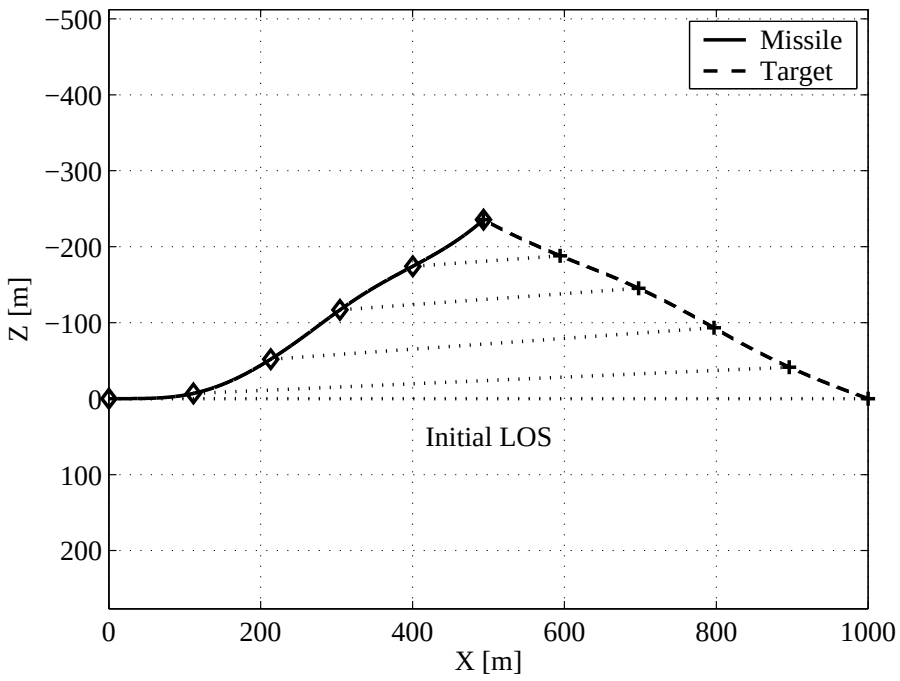

Figure 4. Sample run engagement trajectories.

The missile and target model parameters are given in Table 1. The functions $f_i(\cdot), i = 1, \ldots, 6$ were chosen to be the standard saturation functions

$$\text{sat}(u) = \begin{cases} U_m & u > U_m \\ u & |u| \leq U_m \\ -U_m & u < -U_m \end{cases} \tag{55}$$

with $U_m = 25^\circ$ for all i. Moreover, the fins' deflections were limited to $\pm 25^\circ$. For the controller design, the model functions $\bar{f}_4(\cdot)$ and $\bar{f}_6(\cdot)$, that have to be differentiated with respect to their argument (see Eq. (43)), were chosen as smooth approximations of Eq. (55).

Table 1. Simulation Parameters

Missile		Target
Actual	Model	
$V_M = 380$ m/sec	$\bar{L}_\alpha^B = 1190$ m/sec^2	$V_E = 380$ m/sec
$\tau_c = 0.02$ sec	$\bar{L}_{\delta_c} = 40$ m/sec^2	$a_E^{\max} = 15$ g
$\tau_t = 0.02$ sec	$\bar{L}_{\delta_t} = 40$ m/sec^2	$\Delta T = 1$ sec
	$\bar{M}_\alpha^B = -100\,\text{sec}^{-2}$	$\Delta\phi \in [0, 1]$ sec
	$\bar{M}_q = -5\,\text{sec}^{-1}$	$\tau_E \in [0.05, 0.2]$ sec
	$\bar{M}_{\delta_c} = 80\,\text{sec}^{-2}$	
	$\bar{M}_{\delta_t} = -80\,\text{sec}^{-2}$	

B. Sample Run Performance

The performance of the proposed guidance and control design is first evaluated for a sample run. The target maneuver was characterized by $\tau_E = 0.1$ sec and $\Delta\phi = 0$ sec. In Figs. 5 the ZEM and σ_M, computed using

Eq. (33) and Eq. (35), respectively, are shown. The missile and target accelerations are given in Fig. 6; and the canard and tail deflection angles are plotted in Fig. 7. The initial ZEM error, caused by the heading error, is decreased and maintained close to the desired surface, i.e., $Z = 0$, up to interception. Deviations from the second surface occur as a result of tail saturation, evident in Fig. 7. This happens when high accelerations are generated (see Fig. 6) in order to close the initial heading error and account for the target evasive maneuvers. When the tail is not saturated, the sliding variable σ_M remains close to zero, e.g., in the times interval of $1.05 - 1.25$ sec. The ZEM surface is maintained mainly due to the effect of the canard control. This is possible since the second surface (σ_M) does not explicitly restrict the canard control. Note that strong activity of the canard control is required in order to achieve this task.

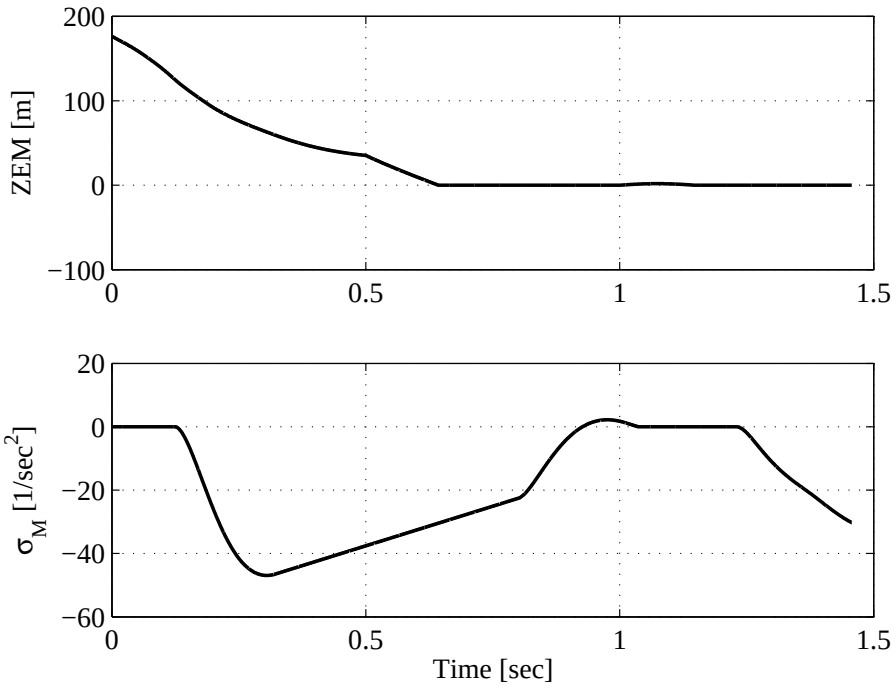

Figure 5. ZEM and σ_M for a sample run.

It is interesting to examine the effect of μ_2 of Eq. (51) on the controller performance. Increasing μ_2 emphasizes the reduction of the flight control motivated sliding variable σ_M. This increase, in effect, increases the missile damping and may improve the interception accuracy. Such a comparison is depicted in Figs. 8. For this sample case, choosing $\mu_2 = [10, 50, 100]$ results in miss distances of 8, 3 and 3.5cm, respectively. This means that choosing a relatively high μ_2 could, on top of providing increased missile damping, over emphasize σ_M on the account of the ZEM surface and hence degrade the interception accuracy.

C. Homing Performance

The homing performance of the proposed algorithm is evaluated by a Monte Carlo simulation study consisting of 100 sample runs for each test point. In these simulations, for each test case, the random variable was chosen as the maneuver phase $\Delta\phi$ of the target, assumed to be distributed uniformly as $\Delta\phi \sim U(-.5, .5)$ sec. The mean and standard deviation of the miss distance are shown in Fig. 9 and Fig. 10 as a function of the target time constant. As can be expected, the miss distance increases as the target time constant decreases. The plots show the results for various values of μ_2, the gain of the uncertainty controller of the second control surface. Similar to the results presented earlier, increasing μ_2 up to a certain level improves the missile dynamic characteristics and consequently the interception accuracy.

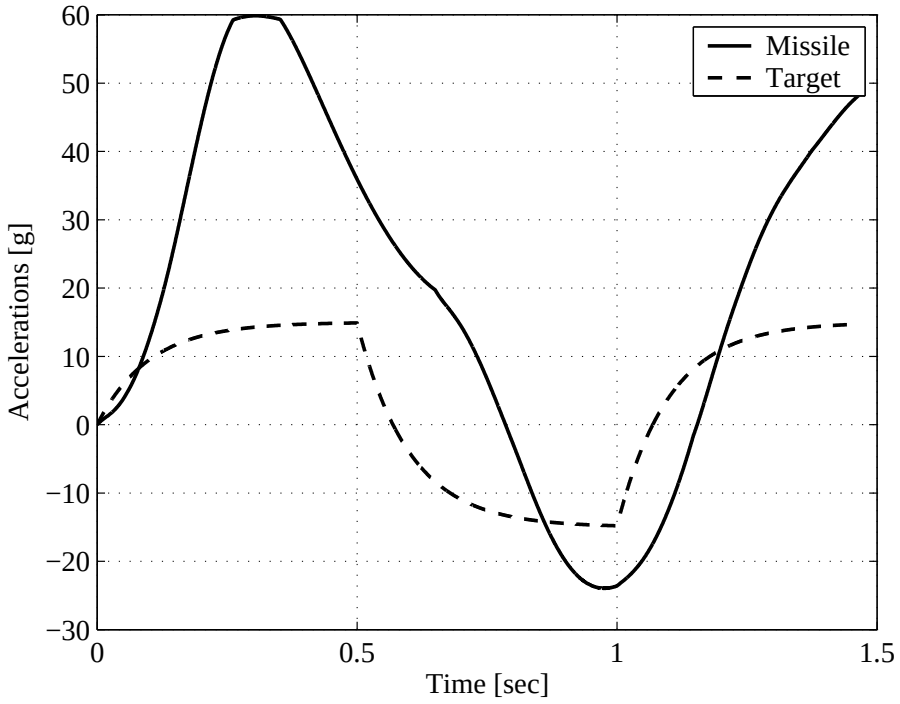

Figure 6. Missile and target acceleration profiles for a sample run.

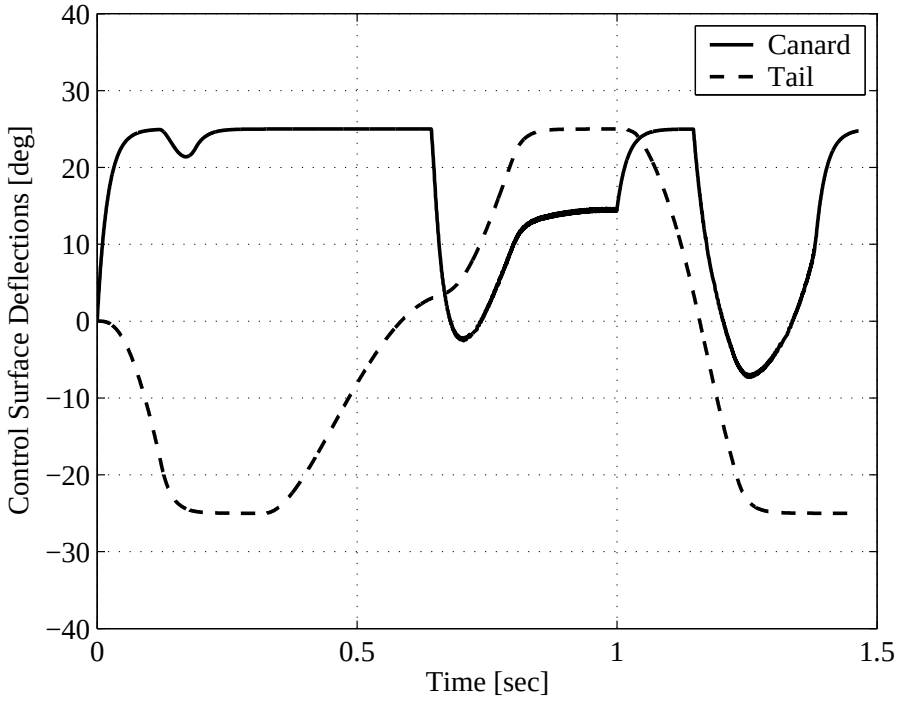

Figure 7. Canard and tail deflections for a sample run.

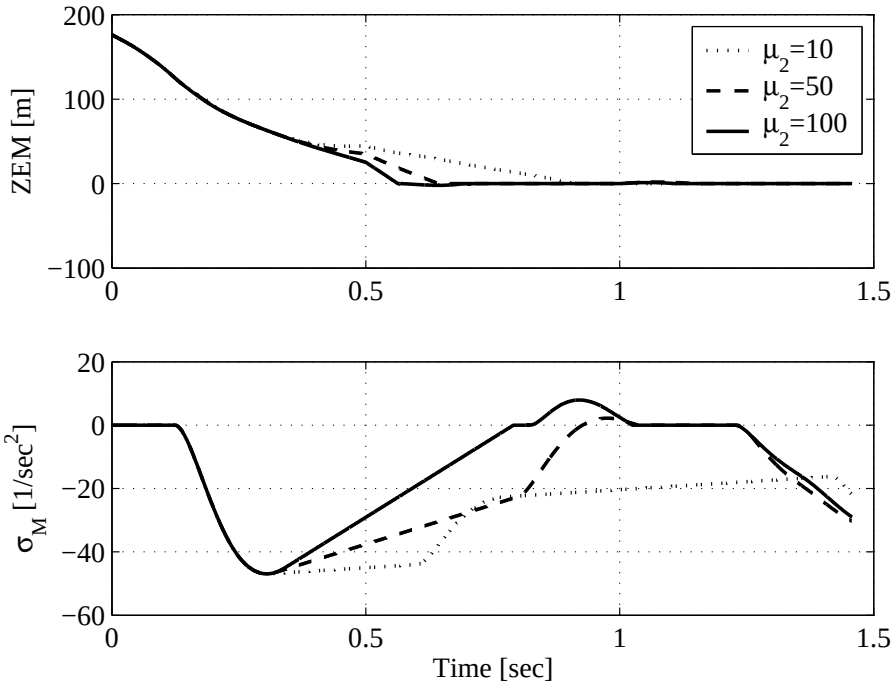

Figure 8. ZEM and σ_M for a sample run and different μ_2 values.

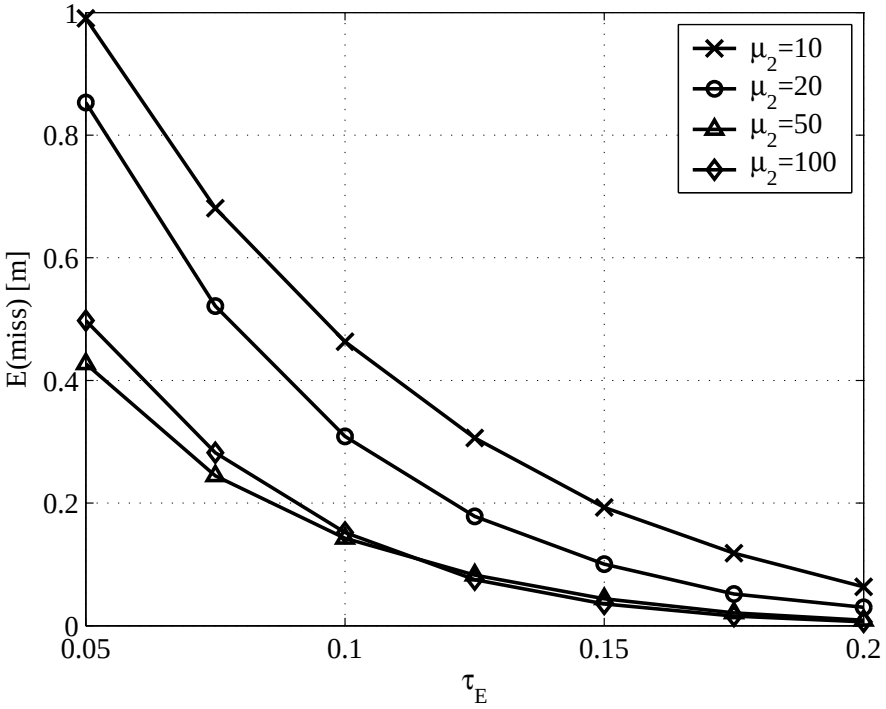

Figure 9. Homing performance evaluation using expected miss.

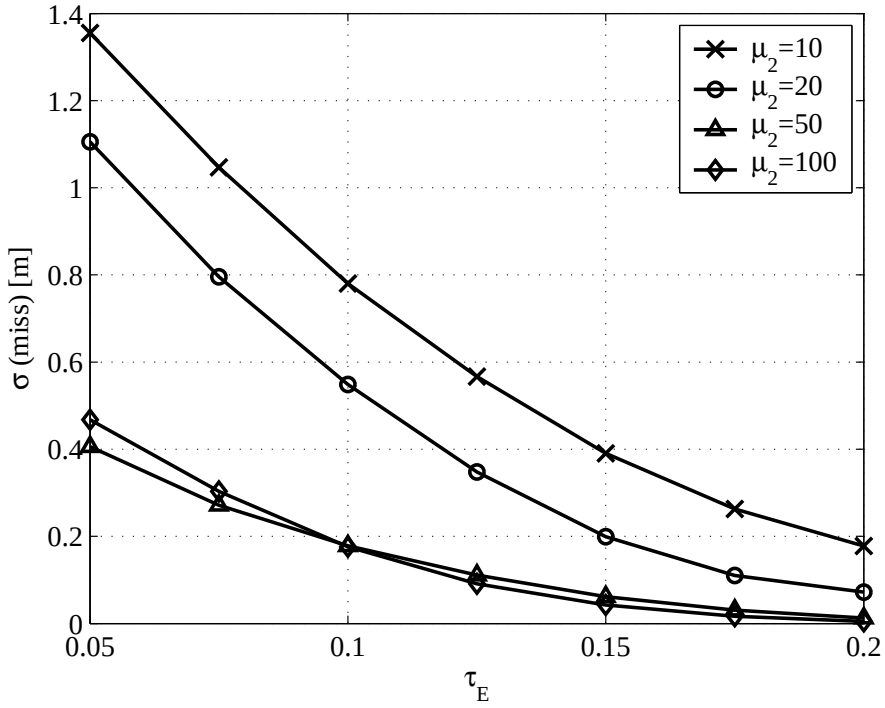

Figure 10. Homing performance evaluation using miss standard deviation.

V. Summary

The sliding mode control approach was used to derive an integrated guidance-control algorithm for a dual control interceptor missile. For this two input control problem, two sliding surfaces were defined. The zero-effort miss distance, from a differential game formulation of the interception problem, was used as one of those sliding surfaces. The additional surface was chosen based on flight-control considerations. The interaction between the two surfaces was investigated. Through Monte Carlo simulations it was shown that small miss distances can be achieved even in stringent interception scenarios.

References

[1]Gutman, S., "Superiority of Canards in Homing Missiles," *IEEE Transactions on Aerospace and Electronic Systems*, Vol. 39, No. 3, 2003, pp. 740–746.

[2]Utkin, V. I., *Sliding Modes in Control and Optimization*, Springer-Verlag, Berlin, 1992.

[3]Slotine, J.-J. E. and Li, W., *Applied Nonlinear Control*, chap. 7, Prentice Hall, Upper Saddle River, NJ, 1991, pp. 276–307.

[4]Bhat, M. S., Bai, D. S., Powly, A. A., Swami, K. N., and Ghose, D., "Variable Structure Controller Design with Application to Missile Tracking," *Journal of Guidance, Control, and Dynamics*, Vol. 24, No. 4, 2001, pp. 859–862.

[5]Thukral, A. and Innocenti, M., "A Sliding Mode Missile Pitch Autopilot Synthesis for High Angle of Attack Maneuvering," *IEEE Transactions on Control Systems Technology*, Vol. 6, No. 3, 1998, pp. 359–371.

[6]Weil, R. D. and Wise, K. A., "Blended Aero and Reaction Jet Missile Autopilot Design using VSS Techniques," *Proceedings of the 30th Conference on Decision and Control*, 1991.

[7]Menon, P. K. and Iragavarapu, V. R., "Adaptive Techniques for Multiple Actuator Blending," *Proceedings of the AIAA Guidance, Navigation, and Control Conference*, CP-4494, AIAA, Washington, DC, 1998.

[8]Manabe, S., "Application of Coefficient Diagram Method to Dual-Control-Surface Missile," *Proceedings of the 15th IFAC Symposium on Automatic Control in Aerospace*, 2001, pp. 499–5042.

[9]Shima, T. and Golan, O. M., "Linear Quadratic Guidance Laws for Missiles with Dual Control Systems," *Proceeding of the AIAA Guidance, Navigation, and Control Conference*, AIAA, Washington, DC, 2002.

[10]Shima, T. and Golan, O. M., "Bounded Differential Game Guidance Law for a Dual Controlled Missile," To appear in: *IEEE Transactions on Control Systems Technology*, 2005.

[11]Shima, T. and Golan, O. M., "End-Game Guidance Laws for Dual Control Missiles," *IMechE Journal of Aerospace Engineering*, Vol. 219, No. 2, 2005, pp. 157–170.

[12]Lin, C. F., Wang, Q., Speyer, J. L., Evers, J. H., and Cloutier, J. R., "Integrated Estimation, Guidance, and Control System Design using Game Theoretic Approach," *Proceedings of the American Control Conference*, American Automatic Control Council, Evanston, IL, 1992, pp. 3220–3224.

[13]Khalil, H. K., *Nonlinear Systems*, chap. 13, Prentice Hall, Upper Saddle River, NJ, 3rd ed., 2002.

[14]Menon, P. K., Sweriduk, G. D., and Ohlmeyer, E. J., "Optimal Fixed-Interval Integrated Guidance-Control Laws for Hit-to-Kill Missiles," *Proceeding of the AIAA Guidance, Navigation, and Control Conference*, CP-5579, AIAA, Washington, DC, 2003.

[15]Palumbo, N. F. and Jackson, T. D., "Integrated Missile Guidance and Control: A State Dependent Riccati Differential Equation Approach," *Proceedings of the IEEE International Conference on Control Applications*, IEEE Press, Piscataway, NJ, 1999, pp. 243–248.

[16]Shkolnikov, I., Shtessel, Y. B., and Lianos, D., "Integrated Guidance-Control System of a Homing Interceptor: Sliding Mode Approach," *Proceeding of the AIAA Guidance, Navigation, and Control Conference*, CP-4218, AIAA, Washington, DC, 2001.

[17]Shima, T., Idan, M., and Golan, O. M., "Sliding Mode Control for Integrated Missile Autopilot-Guidance," *Proceeding of the AIAA Guidance, Navigation, and Control Conference*, AIAA, Washington, DC, 2004.

[18]Zarchan, P., *Tactical and Strategic Missile Guidance*, Vol. 176, Progress in Astronautics and Aeronautics, AIAA, Washington D.C., 1997.

[19]Blakelock, J. H., *Automatic Control of Aircraft and Missiles*, John Wiley & Sons, Inc., New York, NY, 2nd ed., 1991.

[20]Shima, T., "Capture Conditions in a Pursuit-Evasion Game between Players with Biproper Dynamics," To appear in: *Journal of Optimization: Theory and Application*, Vol. 126, No. 3, 2005.

[21]Friedland, B., *Control System Design: An Introduction to State Space Methods*, McGraw-Hill, New York, NY, 1986, pp. 247–248.